# Numerical Modeling and Spectral Balancing of an LED-Based Reflectance Spectrophotometer (360–760 nm)

**Mikhail E. Parfyonov*** **and Dmitry N. Artemyev**
Samara National Research University, 34 Moskovskoe shosse, Samara, 443086, Russian Federation
*e-mail: m.parfyonov@icloud.com

**Abstract.** This study presents numerical modeling and constrained spectral balancing of a compact LED-based reflectance spectrophotometer operating in the 360–760 nm range. The detected spectral response was modeled as a weighted superposition of individual LED emission spectra explicitly multiplied by the wavelength-dependent detector quantum efficiency $QE(\lambda)$. In the baseline configuration with unit weights, the detected spectrum exhibited strong modulation, characterized by a coefficient of variation CV of 41.5%, peak-to-peak deviation of 131%, and maximum-to-minimum ratio of 4.24. Spectral balancing was formulated as a constrained minimization of the normalized variance over a 0.5 nm wavelength grid using a differential evolution algorithm with bounded non-negative weights. The optimized configuration reduced CV to 8.36%, peak-to-peak deviation to 32.2%, and max/min ratio to 1.39, corresponding to an approximately 80% reduction in global spectral non-uniformity as quantified by variance-based metrics. The proposed approach provides a quantitative methodology for spectral equalization in multi-LED reflectance spectrophotometers.

**Keywords:** reflectance spectrophotometry; diffuse reflection; optical design; CCD detector; constrained optimization.

Paper #9513 received 15 Feb 2026; revised manuscript received 6 Apr 2026; accepted for publication 6 Apr 2026; published online 29 Jun 2026. doi: 10.18287/JBPE26.12.020311.

## 1 Introduction

Reflectance spectrophotometry is widely applied for quantitative characterization of materials and functional surfaces through wavelength-resolved analysis of diffusely reflected radiation [1–6]. In biomedical applications, reflectance spectrophotometry provides diagnostically relevant information on tissue condition [7] which motivates further improvement of spectrophotometric systems. In laboratory-scale instruments broadband sources such as tungsten-halogen or xenon lamps are typically employed to provide continuous spectral output. Although such sources ensure broad spectral coverage, they are associated with elevated power consumption, thermal instability, limited lifetime, reduced suitability for compact or field-deployable configurations and some sources exhibit reduced radiant output in the ultraviolet region [8]. The development of solid-state optoelectronics [9–10] has enabled alternative architectures based on discrete light-emitting diodes (LEDs), offering improved energy efficiency, spectral selectivity, and mechanical robustness [11]. In LED-based reflectance systems, broadband coverage is approximated through superposition of multiple emitters with distinct peak wavelengths. However, the aggregate spectral distribution formed by a finite set of LEDs is inherently non-uniform. Moreover, the effective signal registered by the detector is additionally modulated by its wavelength-dependent quantum efficiency. As a consequence, even if the emitted optical power appears approximately balanced at the source level, the detected spectral response may exhibit pronounced variations across the operating range. Such non-uniformity introduces systematic bias in reflectance measurements and reduces comparability between spectral regions; therefore, it is important to ensure uniform illumination, which becomes increasingly difficult as the number of light sources increases [12].

The present work addresses this limitation through numerical modeling and constrained spectral balancing of a compact LED-based reflectance spectrophotometer operating in the 360–760 nm range.

This paper was presented at the XXIII All-Russian Samara Youth Competition and Conference on Optics, Laser Physics and Plasma Physics, Samara, Russian Federation, November 11 – 15, 2025.

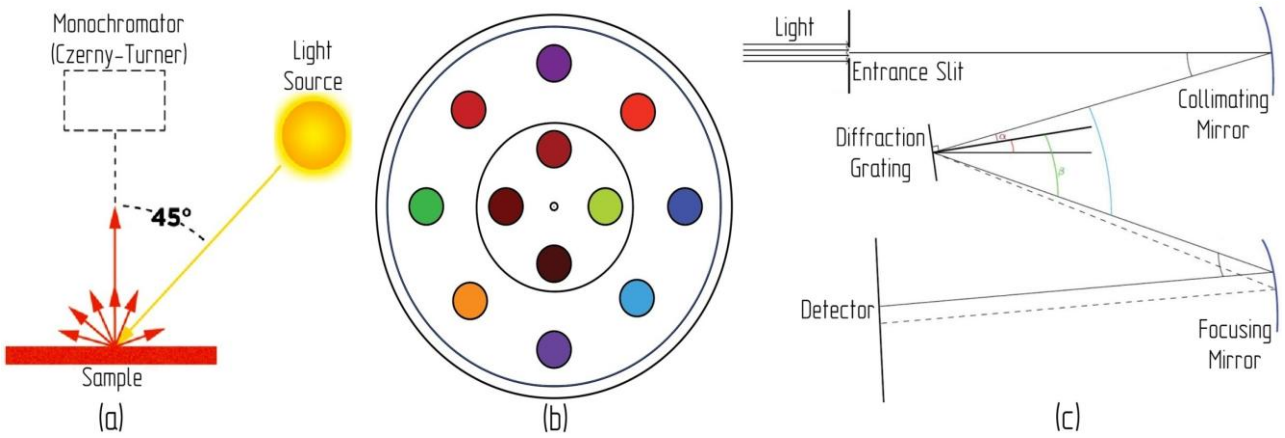


Fig. 1 Optical configuration of the proposed reflectance spectrophotometer, including (a) measurement geometry, (b) illumination system, and (c) spectral dispersion module based on a Czerny-Turner monochromator.

The proposed architecture that combines a 45/0 illumination geometry with a fiber-coupled Czerny-Turner monochromator [13] is shown in Fig. 1(a).

To realize broadband excitation within this configuration, a set of twelve commercially available LEDs with peak wavelengths distributed from the near-ultraviolet to the near-infrared domain is employed. The illumination module is conceptualized as a concentric dual-ring LED arrangement centered on the optical axis of the system and is shown in Fig. 1(b). In addition, to mitigate thermal accumulation, the highest-power LEDs can be spatially distributed across different regions of the array rather than concentrated locally. Such a placement strategy reduces localized heat density, promotes more uniform thermal dissipation, and improves overall thermal stability of the illumination module.

The spectrally resolved detection is achieved using a Czerny-Turner monochromator, schematic of which is shown in Fig. 1(c). In this configuration, incident light enters through the entrance slit and is collimated by a concave mirror. The collimated beam is then directed onto a diffraction grating, where angular dispersion occurs according to wavelength. The diffracted light is subsequently collected and focused by a second concave mirror onto the detector plane. The geometry is defined by the incidence ($\alpha$) and diffraction ($\beta$) angles at the grating, as well as the respective reflection angles at the collimating and focusing mirrors, ensuring spectral separation and imaging onto the detector. The optimization of the angular parameters of the present optical configuration lies outside the scope of this study. The initial angular settings that are often used in the pre-optimization stage can be found in study [14].

The detector quantum efficiency is explicitly incorporated through the wavelength-dependent function $QE(\lambda)$ (Fig. 2), enabling estimation of the effective detected spectral response.

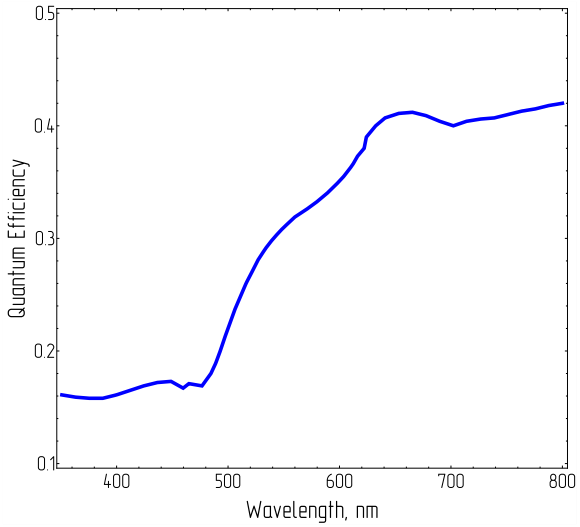


Fig. 2 Quantum Efficiency of a TCD1304DG-UV linear CCD Detector (Toshiba, Japan).

The TCD1304DG-UV linear CCD sensor was selected due to its extended ultraviolet sensitivity and monochrome architecture, which ensure reliable quantum efficiency across the full 360–760 nm spectral range considered in this study. Its high pixel count and 8 µm pixel pitch provide adequate spectral sampling for compact Czerny-Turner configurations, while the absence of a protective cover glass improves short-wavelength transmission. The device also offers straightforward electronic integration, making it suitable for a compact broadband reflectance spectrophotometer.

In the present first-order model, the overall optical throughput of the spectrometer was approximated by a wavelength-independent factor $T \sim 0.5$. This value corresponds to an estimated average transmission of approximately 0.85 per optical element over four sequential components (e.g., fiber coupling, reflective mirrors, diffraction grating efficiency), yielding $0.85^4 \approx 0.52$.

In future work, experimentally measured spectral throughput of the complete optical path will be incorporated as a wavelength-dependent function $T(\lambda)$, allowing more physically accurate modeling and refined optimization of the LED weighting coefficients.

The total detected spectral response is represented as a weighted superposition of individual LED emission spectra multiplied by the detector quantum efficiency. The baseline (pre-optimization) weights $w_i^0$ were initialized uniformly, with all coefficients set to unity, i.e., $w_i^0 = 1$ for all LEDs. This corresponds to an unweighted superposition and serves as a neutral reference prior to optimization. The weighting coefficients are subsequently treated as optimization variables, representing relative drive currents under physically realistic constraints (e.g., non-negativity).

A numerical minimization of the normalized variance of the detected spectrum over a discrete wavelength grid is performed to achieve maximal spectral uniformity within the specified range. The approach enables quantitative comparison between unweighted and optimized configurations using metrics such as coefficient of variation - $CV$, peak-to-peak deviation $P2P_{rel}$, and maximum-to-minimum ratio - $R_{max/min}$.

# 2 Numerical Optimization of Spectral Uniformity

## *2.1 Mathematical Formulation of the Detected Signal*

The detected spectral response of the system was modeled as a weighted superposition of individual LED emission spectra with explicit account of detector quantum efficiency. For a set of *N* LEDs, the spectral signal at the detector plane was written as follows:

$$S(\lambda) = TQE(\lambda) \sum_{i=1}^{N} w_i L_i(\lambda), \quad (1)$$

where $L_i(\lambda)$ stands for the interpolated spectral power distribution of the *i*-th LED obtained from the manufacturer emission profiles. Since the objective was spectral uniformity, the constant *T* does not influence normalized metrics and was therefore retained as a scaling parameter.

All LED spectra and the quantum efficiency curve were reconstructed from tabulated data using cubic interpolation [15]. The operating spectral range was limited to 360–760 nm. For optimization purposes, the wavelength axis was discretized with a step of 0.5 nm, forming a grid $\{\lambda_j\}_{j=1}^{M}$.

The discrete detected signal was then expressed in a vector form as:

$$s_j(\boldsymbol{w}) = QE(\lambda_j) \sum_{i=1}^{N} w_i L_i(\lambda_j), \quad (2)$$

where $\boldsymbol{w} = (w_1, \dots, w_N)^T$ is a vector of optimization variables. Although a wavelength-dependent throughput function is not yet incorporated, it can be introduced multiplicatively into Eq. (2) once experimental transmission data become available.

## *2.2 Objective Function*

Spectral balancing was formulated as a constrained minimization problem. The objective was to reduce the deviation of the detected spectrum from its mean value over the considered wavelength range. The mean signal level was defined as:

$$\mu(\boldsymbol{w}) = \frac{1}{M} \sum_{j=1}^{M} s_j(\boldsymbol{w}), \quad (3)$$

and normalized variance functional was introduced as:

$$J(\boldsymbol{w}) = \frac{1}{\mu(\boldsymbol{w})^2} \sum_{j=1}^{M} \left( s_j(\boldsymbol{w}) - \mu(\boldsymbol{w}) \right)^2. \quad (4)$$

Minimization of $J(\boldsymbol{w})$ corresponds to minimizing the squared coefficient of variation of the detected spectrum. This formulation ensures scale invariance and directly targets spectral flatness rather than absolute signal level.

## *2.3 Constraints and Baseline Configuration*

The initial (baseline) configuration was defined as an unweighted superposition of LED spectra, where every single weight is set to 1.

To reflect practical limitations of current control and optical power adjustment, each weighting coefficient was restricted to an interval $w_i \in [w_i^{(0)} - \Delta w, w_i^0 + \Delta w]$, with physical constraint $w_i \geq 0$. In present model $\Delta w = 1.5$. The constrained formulation prevents unrealistically large compensation of individual spectral regions and ensures physical feasibility of the solution.

## *2.4 Numerical Procedure*

The optimization problem $\min_{w} J(\boldsymbol{w}), 0 \leq w_i \leq \leq 2.5$ was solved numerically using a differential evolution algorithm [16–17]. This population-based global optimization method was selected to reduce sensitivity to local minima arising from partial spectral overlap between adjacent LEDs and non-uniform detector responsivity. A maximum iteration count of 5000 was employed to ensure convergence stability. The optimized weight vector $\boldsymbol{w}^*$ was then used to reconstruct the continuous spectral response $S(\lambda)$ with a 0.5 nm sampling step for visualization and post-analysis.

## *2.5 Evaluation Metrics*

To quantify the degree of spectral equalization achieved through constrained optimization, the baseline and optimized configurations were evaluated using multiple complementary metrics. All metrics were computed over the discrete wavelength grid $\{\lambda_j\}_{j=1}^{M}$ used in the optimization procedure.

The coefficient of variation:

$$CV = \frac{\sigma}{\mu}, \quad (5)$$

provides a normalized measure of spectral non-uniformity that is independent of absolute signal scaling. Since the objective function $J(\boldsymbol{w})$ is proportional to $CV^2$, reduction of $CV$ directly reflects the effectiveness of the optimization process.

To characterize extremal deviations, the normalized peak-to-peak variation was introduced:

$$P2P_{rel} = \frac{S_{max} - S_{min}}{\mu}, \quad (6)$$

where $S_{max} = \max_j s_j$, $S_{min} = \min_j s_j$. This metric captures the full dynamic range of spectral variation relative to the mean level and is particularly sensitive to localized spectral dips or peaks.

Additionally, the maximum-to-minimum ratio:

$$R_{max/min} = \frac{S_{max}}{S_{min}}, \quad (7)$$

was evaluated as a dimensionless indicator of spectral flatness. Unlike variance-based metrics, this ratio directly reflects worst-case deviation and is therefore relevant for applications requiring bounded systematic error across the spectral range.

The simultaneous use of statistical ($CV$), range-based ($P2P$), and extremal (max/min ratio) measures ensures robust characterization of spectral uniformity. Agreement among these metrics confirms that the observed improvement is not confined to a limited portion of the wavelength range but represents global flattening of the detected spectral response.

## 3 Results

The illumination assembly comprises twelve commercially available LEDs with nominal peak wavelengths at 365, 385, 430, 480, 535, 568, 600, 635, 680, 700, 740, and 765 nm. Manufacturer-provided spectral data were used to obtain continuous spectral representations $L_i(\lambda)$ via cubic interpolation to ensure smooth reconstruction over the 360–760 nm range. The aggregate emitted spectrum was initially constructed as an unweighted superposition, corresponding to equal relative drive currents for all channels.

Direct summation of the unweighted spectra produced a strongly modulated aggregate profile, characterized by pronounced local maxima at the individual LED emission peaks and reduced intensity in inter-peak regions where spectral overlap was limited. This behavior is inherent to discrete multi-source architectures, where finite spectral bandwidths and unequal peak intensities prevent natural formation of a flat broadband distribution. When multiplied by the detector quantum efficiency $QE(\lambda)$, the modulation became further amplified. In particular, spectral regions coinciding with high detector responsivity were disproportionately emphasized, whereas regions of reduced quantum efficiency experienced additional attenuation. As a consequence, the baseline detected spectrum exhibited substantial non-uniformity across the 360–760 nm range, even though the nominal spectral coverage of the LED set was continuous.

To visualize the initial spectral behavior of the system, Fig. 3 presents the individual LED emission profiles, the detector quantum efficiency curve $QE(\lambda)$, and the resulting aggregate responses prior to optimization.

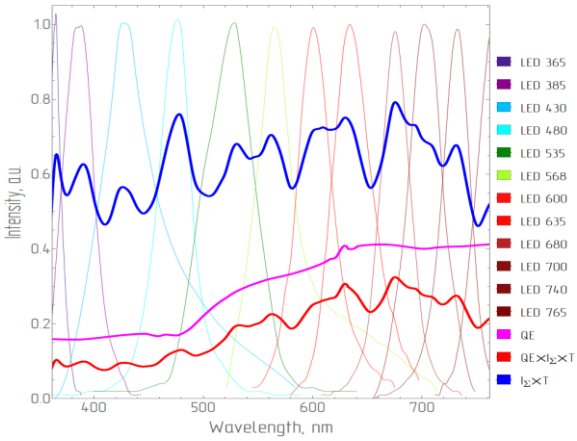


Fig. 3 Individual LED emission spectra, detector quantum efficiency, and baseline detected response prior to spectral optimization.

Fig. 3 illustrates that even after accounting for the uniform throughput factor, the aggregate spectrum remains strongly modulated.

To reduce the observed spectral modulation, a constrained numerical optimization of the LED weighting coefficients $w_i$ was performed. The detected signal was reformulated as stated in Eq. (1), and the weighting coefficients were obtained through constrained minimization of the normalized variance functional described in Section 2. The optimization was carried out over the 360–760 nm range using bounded non-negative weights to preserve physical feasibility with respect to practical current control limitations. The optimized weight vector was determined by minimizing the objective functional within predefined bounds and was found to be $\boldsymbol{w}^* = (2.193, 2.175, 2.500, 1.584, 0.977, 0.851, 0.872, 0.700, 0.651, 0.733, 0.772, 1.146)$, corresponding to the LEDs at 365, 385, 430, 480, 535, 568, 600, 635, 680, 700, 740, and 765 nm, respectively. The resulting weighting distribution reflects the non-uniform spectral sensitivity of the system and compensates for both LED emission characteristics and detector QE variations. This redistribution leads to a more balanced aggregate spectrum prior to final evaluation.

The reconstructed detected spectrum obtained using these optimized coefficients is presented in Fig. 4. Although Fig. 4 provides a complete representation of

the illumination subsystem, including the individual LED emission spectra, the large dynamic range associated with the discrete emission peaks dominates the vertical scale of the plot. As a result, the aggregate detected responses $S(\lambda)$ become visually compressed, and subtle variations between the baseline and optimized spectra are partially masked. This scaling effect reduces the interpretability of global spectral flattening and obscures the quantitative impact of the optimization procedure.

For clarity of analysis and to enable direct visual assessment of spectral uniformity, Fig. 5 therefore presents only the QE-scaled detected responses before and after optimization, without the individual LED components.

Fig. 5 demonstrates that numerical optimization of the LED weighting coefficients significantly reduces spectral modulation of the detected response. In the baseline configuration (red curve), the signal exhibits pronounced amplitude variations across the 360–760 nm range, whereas the optimized spectrum (blue curve) shows markedly improved uniformity and a substantially lower maximum-to-minimum ratio. The optimized profile remains broadband while exhibiting reduced peak dominance and attenuated trough depth, confirming effective redistribution of optical power among the LED channels.

While the graphical comparison visually indicates substantial reduction of spectral modulation after optimization, a quantitative assessment (see Section 2) is required to rigorously evaluate the degree of equalization achieved. The statistical and extremal metrics introduced above were therefore computed for both the baseline and optimized configurations over the same discrete wavelength grid used in the optimization procedure. The calculated values of the coefficient of variation CV, normalized peak-to-peak deviation $P2P_{rel}$, maximum-to-minimum ratio $R_{max/min}$ demonstrate significant improvement in spectral uniformity following constrained optimization. Variance-based measures and extremal metrics show coherent reduction, confirming that the observed flattening is not limited to isolated spectral regions but reflects global redistribution of optical power across the full operating range. Direct numerical comparison of these metrics for the baseline and optimized configurations is summarized in Table 1.

These results confirm the utility of constrained numerical spectral balancing for compact multi-LED reflectance systems and provide quantitative evidence supporting the proposed procedure.

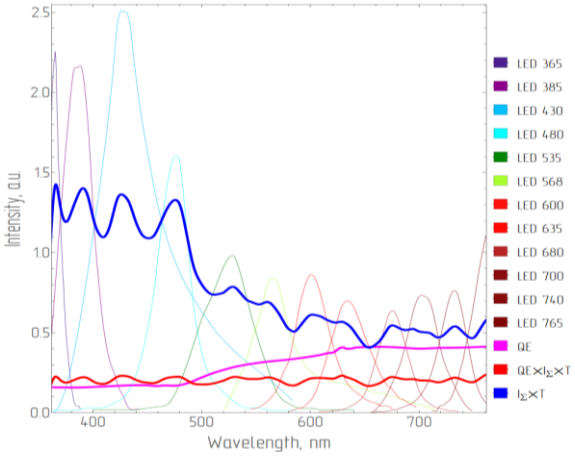


Fig. 4 Individual LED emission spectra, detector quantum efficiency, and detected response after optimization.

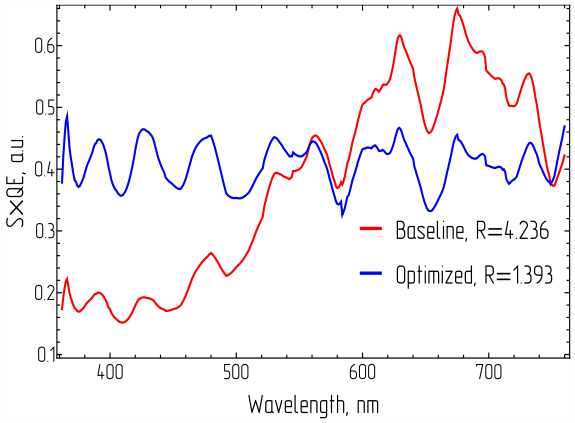


Fig. 5 S×QE, a. u. modeled detected signal with baseline (red) and optimized (blue) weights.

## 4 Conclusion

This study has developed and numerically validated a constrained optimization framework for spectral equalization in a compact LED-based reflectance spectrophotometer operating over the 360–760 nm range. The proposed architecture integrates discrete multi-wavelength LED illumination, a 45/0 diffuse reflectance geometry, and a fiber-coupled Czerny-Turner monochromator, with explicit incorporation of detector quantum efficiency into the forward model of the detected signal.

Table 1 Quantitative comparison of baseline and optimized spectral uniformity metrics.

| Metric | Baseline | Optimized | Relative reduction |
|---|---|---|---|
| $CV$ | 41.46% | 8.36% | 79.8% |
| $P2P_{rel}$ | 131.72% | 32.20% | 75.6% |
| $R_{max/min}$ | 4.236 | 1.393 | 67.1% |

The analysis demonstrates that broadband spectral coverage achieved through discrete emitters does not guarantee uniform detected response. The combined spectral structure of LED emission profiles and wavelength-dependent detector responsivity inherently produces systematic modulation of the measured signal.

This observation highlights a fundamental limitation of source-level balancing approaches that neglect detector characteristics. By formulating spectral equalization as a constrained minimization of normalized variance, the present work establishes a scale-invariant optimization criterion directly linked to statistical measures of spectral uniformity.

The imposed bounds on LED weighting coefficients ensure physical realizability, while the use of a global differential evolution algorithm provides robust convergence under partial spectral overlap between channels. Quantitative evaluation confirmed substantial suppression of spectral non-uniformity across the full operating range.

Beyond the specific numerical results, the principal contribution of this work lies in the explicit coupling of illumination synthesis and detector responsivity within a unified optimization framework. The methodology is not restricted to the particular LED set or detector employed and can be extended to alternative wavelength intervals, detector types, or illumination architectures.

Future developments will extend the model toward a complete radiometric description of the measurement system. Incorporation of a wavelength-dependent throughput function $T(\lambda)$, evaluation of diffuse coupling efficiency into the collection fiber, and quantification of residual specular contributions will enable physically rigorous prediction of measurement bias. In parallel, parametric optimization of the dispersive subsystem under constraints of spectral resolution, optical throughput, and mechanical compactness will facilitate integrated opto-mechanical co-design.

From a practical implementation perspective, the obtained results indicate that spectral uniformity in multi-LED reflectance systems can be achieved through control of individual LED drive currents without modification of the optical layout. This follows directly from the fact that the detected spectral response is formed as a linear superposition of emitter contributions weighted by controllable coefficients.

As a result, compact spectrophotometric devices can be calibrated post-assembly by adjusting channel weights using measured emission spectra and detector responsivity functions. In practical implementations, it is therefore advisable to (i) ensure independent current control for each LED channel, (ii) incorporate experimentally measured spectral characteristics of both emitters and detector into the optimization procedure, and (iii) account for thermal effects when assigning elevated weights to specific LEDs, since non-uniform power distribution inherently leads to localized heat accumulation and may affect spectral stability.

In comparison with conventional broadband illumination systems based on halogen or xenon lamps, the proposed approach relies on discrete, independently controllable emitters rather than a continuous source spectrum. This architectural difference enables direct redistribution of optical power across the spectral range through numerical optimization, which is not accessible in fixed-spectrum sources without additional optical filtering. At the same time, solid-state emitters are intrinsically associated with lower power consumption, reduced thermal load, and improved mechanical robustness, making them suitable for compact and field-deployable systems.

A detailed quantitative comparison with existing systems requires experimental validation and is therefore beyond the scope of the present work. Nevertheless, the presented results demonstrate that numerical spectral balancing constitutes a physically consistent and scalable approach to achieving broadband spectral uniformity in multi-LED spectrophotometric systems.

The proposed framework thus provides a systematic and extensible foundation for the development and optimization of compact, spectrally balanced, solid-state reflectance spectrophotometers suitable for laboratory and field-deployable applications.

## Disclosures

All authors declare that there is no conflict of interest in this paper.

## Reference


1. T. A. Germer, J. C. Zwinkels, and B. K. Tsai (Eds.), Spectrophotometry: Accurate Measurement of Optical Properties of Materials, vol. 46, Elsevier, Oxford, UK (2014). ISBN: 978-0-12-386022-4.
2. G. Kortüm, Reflectance Spectroscopy: Principles, Methods, Applications, Springer, Berlin, Heidelberg (2012). ISBN: 978-3-642-88073-5.
3. A. Springsteen, Applied Spectroscopy: A Compact Reference for Practitioners, Academic Press, 193–224 (1998). ISBN: 978-0-12-764070-9.
4. I. Badura, M. Dąbski, "Reflectance spectroscopy in geology and soil sciences: literature review," Quaestiones Geographicae 41(3), 157–167 (2022).
5. M. Witteveen, D. J. Faber, H. J. C. M. Sterenborg, T. J. M. Ruers, T. G. Van Leeuwen, and A. L. Post, "Opportunities and pitfalls in (sub)diffuse reflectance spectroscopy," Frontiers in Photonics 3, 964719 (2022).
6. E.W. Ciurczak, B. Igne, J. Workman, and D.A. Burns (Eds.), Handbook of Near-Infrared Analysis, 4th ed., CRC Press, Boca Raton (2021). ISBN: 978-1-35-126988-9.

7. M. B. Wallace, A. Wax, D. N. Roberts, and R. N. Graf, "Reflectance spectroscopy," Gastrointestinal Endoscopy Clinics of North America 19(2), 233–242 (2009).
8. I. T. Young, Y. Garini, H. R. C. Dietrich, W. Van Oel, and G. Liqui Lung, LEDs for fluorescence microscopy, Proceedings of SPIE, 5324, 208 (2004).
9. W. Demtröder, Laser Spectroscopy, Springer, Berlin, Heidelberg (2003). ISBN: 978-3-540-73418-5
10. E. F. Schubert, Light-Emitting Diodes, 2nd ed., Cambridge University Press (2006). ISBN: 978-0-511-79054-6
11. S. Pimputkar, J. S. Speck, S. P. DenBaars, and S. Nakamura, "Prospects for LED lighting," Nature Photonics 3, 180–182 (2009).
12. Y. Ryu, D. D. Baldocchi, J. Verfaillie, S. Ma, M. Falk, I. Ruiz-Mercado, T. Hehn, and O. Sonnentag, "Testing the performance of a novel spectral reflectance sensor, built with light emitting diodes (LEDs), to monitor ecosystem metabolism, structure and function," Agricultural and Forest Meteorology 150(12), 1597–1606 (2010).
13. S. D. Noble, R. B. Brown, and T. G. Crowe, "Design and evaluation of an imaging spectrophotometer incorporating a uniform light source," Review of Scientific Instruments 83(3), 033112 (2012).
14. M. Naeem, T. Imran, M. Hussain, and A. S. Bhatti, "Design simulation and data analysis of an optical spectrometer," Optics 3(3), 304–312 (2022).
15. M. Czerny, A. F. Turner, "Über den astigmatismus bei spiegelspektrometern," Zeitschrift für Physik 61, 792–797 (1930).
16. P. R. Bevington, D. K. Robinson, Data Reduction and Error Analysis for the Physical Sciences, McGraw-Hill Education, (2003). ISBN: 978-0-07-247227-1.
17. R. Storn, K. Price, "Differential evolution – a simple and efficient heuristic for global optimization over continuous spaces," Journal of Global Optimization 11(4), 341–359 (1997).